Arabian Journal of Chemistry (2023) **16**, 104572

King Saud University

Arabian Journal of Chemistry

www.ksu.edu.sa
www.sciencedirect.com

ORIGINAL ARTICLE

Derivatization of dihydrotetrabenazine for technetium-99m labelling towards a radiotracer targeting vesicular monoamine transporter 2

Chunyi Liu, Yi Fang, Jie Tang, Zhengping Chen *

NHC Key Laboratory of Nuclear Medicine, Jiangsu Key Laboratory of Molecular Nuclear Medicine, Jiangsu Institute of Nuclear Medicine, Wuxi, Jiangsu 214063, China

Received 25 September 2022; accepted 9 January 2023
Available online 13 January 2023

KEYWORDS

Dihydrotetrabenazine;
Bisaminobisthiol;
Technium-99m;
Vesicular monoamine transporter 2

Abstract The development of technetium-99m-labelled dihydrotetrabenazine (DTBZ) derivative for vesicular monoamine transporter 2 (VMAT2) tracing could be a benefit for single photon emission computed tomography (SPECT) imaging due to easy labelling chemistry and great availability through nuclide generator system. Here, we successfully prepared a technetium-99m-labelled DTBZ derivative and subsequently evaluated its biological activity targeting VMAT2. A novel combination of the bisaminoethanethiol (BAT) chelator scaffold with the biologically active DTBZ vector was performed to synthesize the labelling precursor BAT-P-DTBZ, and it was accomplished in six steps. The technetium-99m labelling was carried out in the radiochemical study of BAT-P-DTBZ conjugate, and the radiolabelling conditions were investigated and optimized. Under the optimized labelling condition, ^{99m}Tc-BAT-P-DTBZ was acquired with a good radiochemical purity of above 95 %. The quality control test showed that ^{99m}Tc-BAT-P-DTBZ is stable over 6 h and it has a suitable lipophilicity, suggesting successful appositeness for the needs of routine biological evaluation experiments. The *in vitro* biological evaluation revealed that ^{99m}Tc-BAT-P-DTBZ could bind to VMAT2 sites. The *in vivo* biodistribution study clearly indicated that the pancreas (VMAT2-enriched region) displays relatively high uptake of ^{99m}Tc-BAT-P-DTBZ among all organs in mice. The specific VMAT2 binding signal of ^{99m}Tc-BAT-P-DTBZ was separately detected in the *in vitro* and *in vivo* biological evaluation. Therefore, ^{99m}Tc-BAT-P-DTBZ might be a potential imaging agent for monitoring VMAT2 binding sites in the pancreas.

* Corresponding author at: 20 Qianrong Road, Wuxi 214063, PR China.
E-mail address: chenzhengping@jsinm.org (Z. Chen).

Peer review under responsibility of King Saud University.

Production and hosting by Elsevier

https://doi.org/10.1016/j.arabjc.2023.104572
1878-5352

1. Introduction

The vesicular monoamine transporter 2 (VMAT2) is an integral membrane protein that mediates monoamine neurotransmitters (dopamine, serotonin, norepinephrine and histamine) from cellular cytosol into small synaptic and dense core vesicles in the neuronal terminal (Lohr et al., 2015, Cliburn et al., 2017). In the living brain, VMAT2 is highly expressed in the striatum and represents a common target providing information about the neuronal integrity (Hoffman et al., 1998). VMAT2 dysfunction in the brain associates with many neurological and psychiatric disorders, including Parkinson's disease (PD), Alzheimer's disease (AD) and some others (Bernstein et al., 2014). Moreover, immunohistochemical staining of gene expression in the endocrine pancreas demonstrated that VMAT2 binding sites are also expressed mainly on pancreatic β-cells (Maffei et al., 2004). VMAT2 expression matches well with the insulin levels in pancreas tissue and it is related to diabetes mellitus (Harris et al., 2008). Therefore, VMAT2 could also be an excellent target for mapping β-cell function. Recent studies showed that the evaluation of VMAT2 could be achieved by positron emission tomography (PET) or single photon emission computed tomography (SPECT) technique and the VMAT2 imaging is available for early clinical diagnosis, classification and treatment monitoring of the above mentioned diseases (Kilbourn 1997, Simpson et al., 2006).

Recently, a number of VMAT2 PET imaging agents based on dihydrotetrabenazine (DTBZ) or its closely related congeners have been reported (Fig. 1). Initially, tracers were made by labelling DTBZ itself with radionuclide carbon-11 ([^{11}C]DTBZ and [^{11}C](+)-DTBZ) (Frey et al., 1996, Koeppe et al., 1996) and they were confirmed as reliable PET tracers in human subjects to examine the integrity of striatal presynaptic monoaminergic terminals (Chan et al., 1999, Sanchez-Catasus et al., 2021). Since fluorine-18 has a longer half-life than carbon-11 (109.8 vs 20.4 min) and it has an advantage of wider application in research and clinical settings including better suitability for multistep radiolabeling procedures, multiple PET scans with a single production and higher spatial image resolution. Thus, several ^{18}F-labelled DTBZ derivatives have been successfully developed to target VMAT2, such as [^{18}F]FP-DTBZ (Goswami et al., 2006), [^{18}F]FP-(+)-DTBZ (Kung et al., 2007, Lin et al., 2011, Zhao et al., 2020, Liu et al., 2021), [^{18}F]FE-(+)-DTBZ (Eriksson et al., 2010) and [^{18}F]FP-E-(+)-TBZ (Kung et al., 2008a). Among these ^{18}F-labelled tracers, [^{18}F]FP-(+)-DTBZ has been demonstrated a high sensitivity for detecting monoaminergic terminal reductions and proven to be useful for assessing the disease progression of PD in clinical trials (Hsiao et al., 2014). Furthermore, [^{18}F]FP-(+)-DTBZ was also used for β-cell mass estimates in diabetes (Freeby et al., 2016). Along this line, the deuterated ^{18}F-analogs of DTBZ, namely [^{18}F]FP-(+)-DTBZ-d_6 (Liu et al., 2018) and [^{18}F]FE-(+)-DTBZ-d_4 (Nag et al., 2021), were developed to improve metabolic stability, thus serving as optimal tools for *in vivo* applications. In addition, in order to develop a relatively long-lived PET imaging agent for noninvasive assessment of VMAT2 expression, ^{64}Cu-CB-TE2A-(+)-DTBZ was prepared by the radiolabelling DTBZ with nonstandard PET nuclide copper-64 (Kumar et al., 2014). In brief, the utilization of cyclotron produced nuclide (^{11}C, ^{18}F or ^{64}Cu) labelled DTBZ-derived structure for VMAT2 tracing through PET is an advanced imaging technique, however the disadvantage is the fact that ^{11}C, ^{18}F or ^{64}Cu labelled compound should be produced in centers with cyclotron and fully equipped radiochemistry facility.

SPECT is much more widely available than PET owing to its more affordable cost. SPECT radiotracer is generally a bioactive molecule labelled with a gamma-emitting isotope (Eid Moustapha et al., 2016, Shahzad et al., 2019, Shahzadi et al., 2019, Mogadam et al., 2020, Davoodikia et al., 2022, Mogadam et al., 2022). Of the SPECT nuclides currently in use, technetium-99m has become the workhorse of diagnostic nuclear medicine in hospitals worldwide. The wide utilization of technetium-99m is owing to (a) simple and cost-effective availability via a ^{99}Mo/^{99m}Tc generator; (b) medium energy (140 keV) γ-ray with 89 % abundance; (c) practical half-life of 6.02 h; and (d) easier labelling chemistry. SPECT imaging with a technetium-99m radiotracer is an important part in the research domain of nuclear medicine. In this study, we designed and synthesized a technetium-99m-labelled chelator-coupled complex based on the DTBZ lead structure (^{99m}Tc-BAT-P-DTBZ, Fig. 2). The bisaminoethanethiol (BAT) chelator as a verified chelating agent for technetium-99m (O'Neil et al., 1994, Meegalla et al., 1997, Zhuang et al., 1999) was chosen. The biologically active DTBZ vector was connected to the chelator via a chain linker. This report presented chemical synthesis, radiochemical labeling as well as condition optimization, quality control and preliminary biological evaluation of a technetium-99m-labelled DTBZ derivative. The results indicated that ^{99m}Tc-BAT-P-DTBZ could bind to VMAT2 and it has potential application in VMAT2 tracing. Our investigation provided a suitable technetium-99m radiolabeling method for the bioactive DTBZ molecules, and the present study also offered a glimpse into the development of novel technetium-99m-labelled VMAT2 tracers for SPECT.

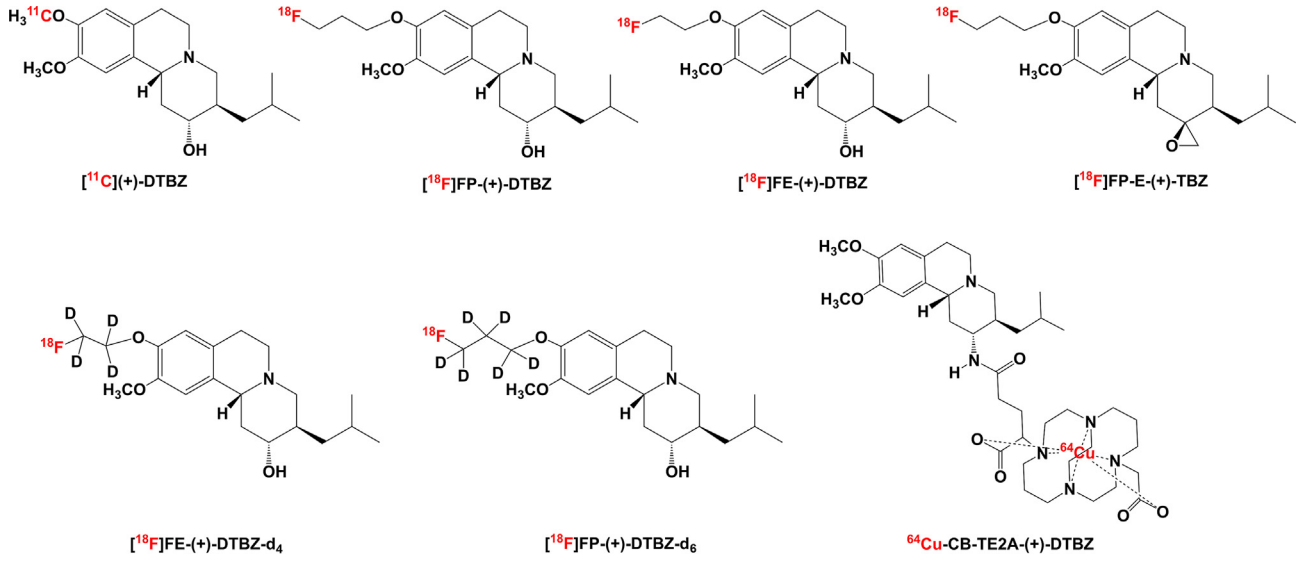

Fig. 1 Representative DTBZ derivates reported for PET imaging of VMAT2.

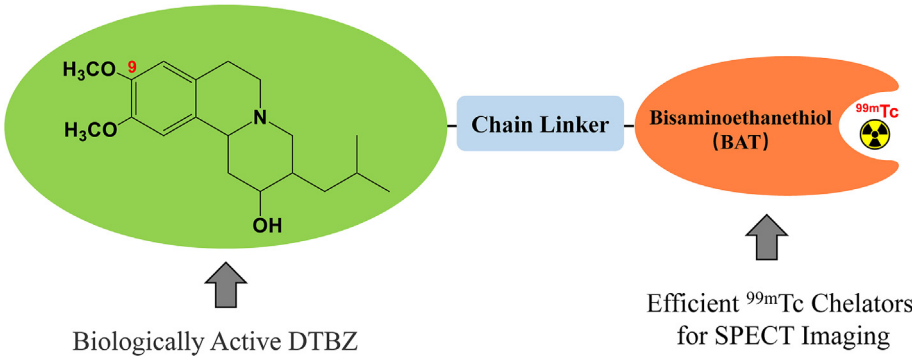

Fig. 2 Design of technetium-99m-labelled DTBZ.

2. Materials and methods

All reagents and solvents were commercial products and were used without further purification unless otherwise mentioned. Dihydrotetrabenazine was synthesized according to literature method (Liu et al., 2012a, Liu et al., 2012b). N-[2″-(p-methoxybenzylmercapto)ethyl]-2-[(2′-(p-methoxybenzylmercapto)ethyl)amino] acetamide (**1**) was produced in our laboratory as previously reported by O'Neil et al (O'Neil et al., 1994). The silica gel used for column chromatography was H type (600 mesh – 800 mesh). MS spectra were recorded on a SQ Detector 2 mass spectrometer (Waters, USA). IR spectra in the range 4000–400 cm-1 were acquired on a Tensor 27 infrared spectrometer (Bruker, Germany). NMR spectra were measured on a Avance III 400 MHz digital NMR spectrometer (Bruker, Germany). Technetium-99m was eluted as $^{99m}TcO_4^-$ from $^{99}Mo/^{99m}Tc$ generator (HTA, China). Radio-HPLC analysis was made in a Waters 1525 Series LC system equipped with a radiomatic 610TR detector (Perkin-Elmer, USA). Measurement of radioactivity was performed in a 2470 automatic gamma (γ) counter (Perkin-Elmer, USA). Centrifugation was carried out by a TDL-60B centrifuge (Anting Scientific, China). Male Sprague-Dawley (SD) rats were provided by Changzhou Cavens Laboratory Animal Co., ltd. The striatum was homogenized by a Scientz-48 high throughput tissue grinder (Scientz, China). All animal experiments were approved by the Animal Care and Ethics Committee of Jiangsu Institute of Nuclear Medicine.

2.1. Synthesis of the precursor for technetium-99m-labelled DTBZ

The synthetic strategy employed for the preparation of the precursor for technetium-99m-labelled DTBZ was illustrated in Scheme 1. The whole synthesis route focused on the connection between biologically active DTBZ vector and chelating group BAT.

*2.1.1. N-[2″-(p-methoxybenzylmercapto)ethyl]-2-[(2′-(p-methoxybenzylmercapto) ethyl)(N'-hydroxypropyl)amino] acetamide (**2**)*

N-[2″-(p-methoxybenzylmercapto)ethyl]-2-[(2′-(p-methoxybenzylmercapto)ethyl) amino] acetamide (**1**) (1.0 g, 2.3 mmol) was dissolved in anhydrous acetonitrile (25 mL), and then 3-bromopropanol (624 μL, 6.9 mmol) and triethylamine (1.6 mL, 11.5 mmol) were added. The mixture was stirred and heated at 90 °C for 24 h under nitrogen. The solvent was removed under reduced pressure. The residue was partitioned between ethyl acetate (50 mL) and water (25 mL). The layers were separated, and the organic extract was concentrated in vacuum. The crude product was purified by column chromatography silica gel ($MeOH/CH_2Cl_2$ 2/100, v/v) to afford 540 mg of compound **2** as pale yellow oil in 47.7 % yield. MS, *m/z*: 494 $[M + H]^+$; 516 $[M + Na]^+$. IR (ν, cm^{-1}): 3332; 2933; 2834; 1657; 1610; 1512; 1463. ^1H NMR ($CDCl_3$, 400 MHz), δ: 7.23~7.18 (m, 4H), 6.85~6.82 (m, 4H), 3.78 (s, 6H), 3.69~3.65 (q, 6H), 3.44~3.39 (q, 2H), 3.04 (s, 2H), 2.65~2.51 (m, 8H), 1.68~1.61 (m, 2H).

*2.1.2. N-[2″-(p-methoxybenzylmercapto)ethyl]-2-[(2′-(p-methoxybenzylmercapto) ethyl)(N'-tosylatepropyl)amino] acetamide (**3**)*

To compound **2** (480 mg, 0.98 mmol) in dry dichloromethane (25 mL), DMAP (239 mg, 1.95 mmol) and triethylamine (272 μL, 1.95 mmol) were added under nitrogen. The mixture was cooled to 0 °C, then p-tosyl chloride (224 mg, 1.17 mmol) was added and the mixture was stirred overnight at room temperature. Next, distilled water (25 mL) was added and the layers were separated. The aqueous phase was extracted with dichloromethane (3 × 20 mL). The combined organic extracts were dried over Na_2SO_4, evaporated and purified by column chromatography silica gel ($MeOH/CH_2Cl_2$ 1/100, v/v) to give 410 mg of compound **3** in 64.7 % yield. MS, *m/z*: 647 $[M + H]^+$; 669 $[M + Na]^+$. IR (ν, cm^{-1}): 3338; 2933; 2835; 1672; 1610; 1512; 1463. ^1H NMR ($CDCl_3$, 400 MHz), δ: 7.77 (d, J = 8.28 Hz, 2H), 7.65~7.62 (m, 1H), 7.32 (d, J = 8.06 Hz, 2H), 7.23~7.18 (m, 4H), 6.85~6.83 (m, 4H), 4.08 (t, J = 6.04 Hz, 2H), 3.79 (s, 3H), 3.78 (s, 3H), 3.65 (s, 2H), 3.63 (s, 2H), 3.42~3.37 (m, 2H), 2.99 (s, 2H), 2.59 (t, J = 6.71 Hz, 2H), 2.53 (t, J = 6.62 Hz, 4H), 2.50~2.47 (m, 2H), 2.44 (s, 3H), 1.76~1.71 (m, 2H).

*2.1.3. 9-Desmethyl-dihydrotetrabenazine (**5**)*

N-methylaniline (438 μL, 4 mmol) was added dropwise at 95 °C to a stirred suspension of 80 % sodium hydride (400 mg, 16 mmol) and hexamethylphosphoramide (700 μL, 4 mmol) in dry xylene (20 mL) under nitrogen. After 15 min, dihydrotetrabenazine (4) (638 mg, 2 mmol) was added to the above mixture. The suspension was stirred for 48 h at 95 °C. The reaction mixture was cooled to room temperature, and

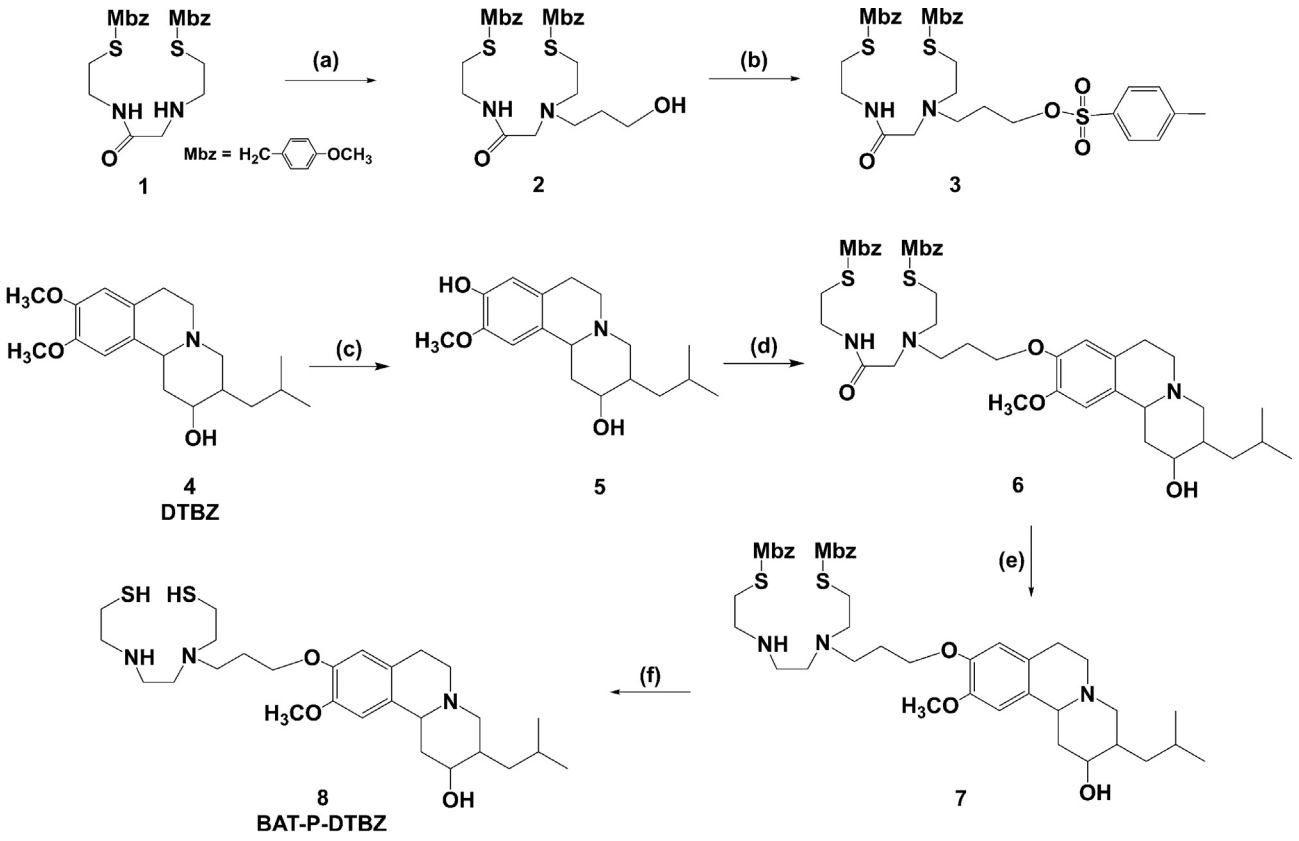

Scheme 1 Synthesis of the precursor for ^{99m}Tc-BAT-P-DTBZ. (a) 3-Bromopropanol, Et_3N, CH_3CN, 90 °C, 24 h. (b) p-Tosyl chloride, DMAP, Et_3N, CH_2Cl_2, 0 °C to room temperature, overnight. (c) NaH, HMPA, *N*-methylaniline, xylene, 95 °C, 48 h. (d) Compound **3**, Cs_2CO_3, DMF, 120 °C, 24 h. (e) 1 M Borane-THF, 80 °C, overnight. (f) TFA, anisole, methanesulfonic acid, 0 °C to room temperature, 1 h.

then 20 % sodium hydroxide aqueous solution (50 mL) was added slowly with stirring. The aqueous phase was separated and washed several times with ether. Next, the aqueous phase was neutralized by 6 M of HCl until the pH reached 7 – 9 and extracted with ether (3 × 50 mL). The combined organic extracts were dried over Na_2SO_4, evaporated and purified by column chromatography silica gel (MeOH/CH_2Cl_2 4/100, v/v). Yield of 9-desmethyl-dihydrotetrabenazine was 460 mg (75.4 %). MS, *m/z*: 306.2 $[M + H]^+$; 288.2 $[M-OH]^+$; 260.1 $[M-C2H5O]^+$. IR (ν, cm^{-1}): 3099; 2949; 1609; 1529; 1463. ^{1}H NMR ($CDCl_3$, 400 MHz), δ: 6.74~6.55 (m, 2H), 5.47 (s, 1H), 3.84 (s, 3H), 3.41~3.36 (m, 1H), 3.14~2.97 (m, 4H), 2.64 (d, J = 9.27 Hz, 2H), 2.59~2.50 (m, 2H), 2.48~2.42 (m, 1H), 1.98 (t, J = 11.0 Hz, 1H), 1.73~1.61 (m, 3H), 1.09~1.02 (m, 1H), 0.94 (d, J = 6.52 Hz, 3H), 0.91 (d, J = 6.59 Hz, 3H).

*2.1.4. p-Methoxybenzyl-monoaminomonoamidedithiol-propyl-dihydrotetrabenazine (**6**)*

To a yellow solution of compound **5** (198 mg, 0.65 mmol) in absolute DMF (20 mL), cesium carbonate (635 mg, 1.95 mmol) was added. The mixture was stirred for 30 min at room temperature. A DMF (5 mL) solution of compound 3 (420 mg, 0.65 mmol) was then added to the resultant orange solution. The mixture was stirred at 120 °C for 24 h under nitrogen, during which the solution turned dark red. The solvent was removed under reduced pressure. The residue was partitioned between ethyl acetate (50 mL) and water (25 mL). The layers were separated. The organic phase was dried over Na_2SO_4 and concentrated in vacuum. The crude product was purified by column chromatography silica gel (MeOH/EtOAc 2/100, v/v) to obtain 180 mg of compound 6 as yellowish oil in 35.5 % yield. MS, *m/z*: 781 $[M + H]^+$; 803 $[M + Na]^+$. IR (ν, cm^{-1}): 3335; 2952; 2920; 2868; 2835; 1664; 1609; 1512; 1464. ^{1}H NMR ($CDCl_3$, 400 MHz), δ: 7.86~7.77 (m, 1H), 7.20~7.15 (dd, 4H), 6.83~6.81 (d, 4H), 6.67 (s, 1H), 6.59 (s, 1H), 4.03~4.00 (m, 1H), 3.92~3.90 (d, 1H), 3.79~3.77 (d, 9H), 3.61~3.59 (d, 4H), 3.41~3.33 (m, 3H), 3.12~2.96 (m, 6H), 2.69~2.63 (m, 5H), 2.54~2.41 (m, 6H), 1.99~1.90 (m, 6H), 1.62~1.55 (m, 1H), 1.52~1.43 (m, 1H), 1.09~1.01 (m, 1H), 0.94 (d, J = 6.50 Hz, 3H), 0.92 (d, J = 6.47 Hz, 3H).

*2.1.5. p-Methoxybenzyl-bisaminodithiol-propyl-dihydrotetrabenazine (**7**)*

Compound **6** (300 mg, 0.38 mmol) was added to 1 M borane-tetrahydrofuran solution (7.6 mL, 7.6 mmol) under nitrogen, and the resulting mixture was heated at reflux overnight. The reaction mixture was cooled to 0 °C, and distilled water was added dropwise until no more gas evolution was observed, and then the mixture was concentrated in vacuo. The residue was added to a mixture of ethanol (20 mL) and 1 M hydrochloric acid (20 mL) and hydrolyzed at 60 °C for 3 h.

The solution was then basified with concentrated NH_4OH. The product was extracted into CH_2Cl_2 and purified by column chromatography silica gel (MeOH/EtOAc 1/9, v/v) to produce compound **7** (70 mg, 24 %). MS, *m/z*: 767.3 $[M + H]^+$; 788.7 $[M + Na]^+$. IR (v, cm^{-1}): 3356; 2951; 2834; 1610; 1511; 1464. ^1H NMR ($CDCl_3$, 400 MHz), δ: 7.20~7.18 (d, 4H), 6.83~6.80 (dd, 4H), 6.71~6.57 (m, 2H), 4.05~3.99 (m, 2H), 3.80 (s, 3H), 3.78~3.76 (d, 6H), 3.63~3.60 (d, 4H), 3.41~3.35 (m, 1H), 3.12~3.10 (br. d, 1H), 3.05~2.96 (m, 3H), 2.76~2.72 (m, 2H), 2.65~2.64 (br. d, 2H), 2.62~2.58 (m, 8H), 2.56~2.52 (m, 4H), 2.46~2.39 (m, 2H), 1.99~1.96 (d, 2H), 1.94~1.87 (m, 2H), 1.75~1.65 (m, 2H), 1.61~1.55 (m, 1H), 1.52~1.43 (m, 1H), 1.10~1.02 (m, 1H), 0.94 (d, J = 6.49 Hz, 3H), 0.92 (d, J = 6.46 Hz, 3H).

2.1.6. Bisaminodithiol-propyl-dihydrotetrabenazine (*8*)

Compound **7** (70 mg, 0.09 mmol) was dissolved in trifluoroacetic acid (2.1 mL) and anisole (31 μL) at 0 °C, and methanesulfonic acid (310 μL) was added. The resulting mixture was stirred for 1 h under nitrogen and concentrated in vacuo to obtain a viscous oil. Distilled water (15 mL) was then added to the above oil at 0 °C, and the resulting suspension was washed several times with ether (3 × 15 mL). The aqueous phase was basified by sodium bicarbonate and extracted with dichloromethane (2 × 15 mL). The combined organic extracts were dried over Na_2SO_4. Next, dry HCl gas was passed through the above organic phase for 2 min and the organic phase was concentrated in vacuo to obtain the hydrochloride salt of compound **8** (40 mg, 70 %). MS, *m/z*: 526.3 $[M + H]^+$; 492.3 $[M-SH]^+$. HRMS (ESI-TOF): *m/z* $[M + H]^+$ calcd for $C_{27}H_{48}N_3O_3S_2^+$ 526.3137; found 526.3109. ^1H NMR (CD_3OD, 400 MHz), δ: 6.98~6.84 (m, 2H), 4.49~4.46 (br. d, 1H), 4.20 (br. s, 2H), 3.90~3.85 (m, 5H), 3.83~3.55 (m, 11*H*), 3.45~3.36 (m, 4H), 3.05~2.89 (m, 4H), 2.46~2.27 (m, 2H), 2.14~1.89 (m, 2H), 1.83~1.69 (m, 3H), 1.21~1.14 (m, 2H), 1.01 (d, J = 5.95 Hz, 3H), 0.98 (d, J = 5.93 Hz, 3H).

2.2. Radiolabelling procedure

The free ligand (compound **8**) was dissolved in ethanol. An accurate amount of ethanol solution was transferred to a vial. Then, a freshly prepared deoxygenated aqueous mixture containing of stannous chloride ($SnCl_2{\cdot}2H_2O$), sodium glucoheptonate (GH) and disodium edetate (EDTA-2Na) was added. The pH of the mixed solution was adjusted using citric acid-citrate sodium buffer and the total volume of the preparation was approximately 2 mL. ^{99m}Tc-pertechnetate (1 mL, ranging from 37 to 111 MBq) in saline was then added to the above reaction medium and the mixture was heated at 100 °C for 30 min before assessing the radiochemical conversion (RCC) of the technetium-99m-labelled DTBZ complex (^{99m}Tc-BAT-P-DTBZ). The reaction conditions such as the reaction temperature (70–100 °C), the reaction time (5–30 min), EDTA-2Na amount (0.2–2 mg), GH amount (1–25 mg), the pH value of the reaction solution (2–9), the labelling precursor amount (10–200 μg) and $SnCl_2{\cdot}2H_2O$ amount (10–100 μg) were investigated and optimized in order to maximize the radiolabelling efficiency.

The crude ^{99m}Tc-BAT-P-DTBZ product was purified by extraction from the aqueous reaction mixture with dichloromethane and the dichloromethane was removed under a flow of N_2. The residual pure ^{99m}Tc-BAT-P-DTBZ was dissolved in ethanol for standby.

2.3. Quality control of ^{99m}Tc-BAT-P-DTBZ

2.3.1. Radiochemical purity

The radiochemical purity (RCP) of ^{99m}Tc-BAT-P-DTBZ was estimated by high performance liquid chromatography (HPLC) system. Chromatographic analysis was performed on a Waters liquid chromatography system equipped with a 1525 binary HPLC pump and a Radiomatic 610TR detector. A reversed-phase HPLC column (C18, 5 μm, 4.6 × 150 mm, Waters, Symmetry) was employed, and the column temperature was maintained at room temperature. The mobile phase consisted of acetonitrile, water and triethylamine (48: 52: 0.1, v/v/v) was filtered through a 0.45 μm membrane filter and degassed with ultrasound before use. The flow rate of the mobile phase was kept at 1.0 mL/min under isocratic elution. The sample solution (10 μL) was directly injected into the chromatographic system.

2.3.2. Stability test

The stability of freshly produced ^{99m}Tc-BAT-P-DTBZ was performed in phosphate buffer solution (PBS, pH = 7.4) and fetal bovine serum (FBS). An aliquot of ^{99m}Tc-BAT-P-DTBZ (37 MBq) was added to PBS (2.0 mL) and FBS (2.0 mL) respectively, and the *in vitro* incubation was kept at 37 °C. The RCP of ^{99m}Tc-BAT-P-DTBZ was determined by the chromatographic method as mentioned above at 0, 1, 2, 4, and 6 h.

2.3.3. Partition coefficient

Partition coefficient was determined by mixing ^{99m}Tc-BAT-P-DTBZ solution with *n*-octanol and phosphate buffer at room temperature. Two phosphate buffers (pH = 7.0 and 7.4) were adopted for the test respectively. A 10 μL aliquot of ^{99m}Tc-BAT-P-DTBZ (37 MBq/mL) was added into two-phase mixture of 3 mL *n*-octanol and 3 mL phosphate buffer. The test tube was vortexed for 5 min and then centrifuged for 5 min. Two pipetted samples (1 mL each) from the *n*-octanol and buffer layers were measured in a gamma counter. Samples from the *n*-octanol layer were repartitioned and all measurements were tested in quadruplicate. The log*P* value was obtained by the formula: $\log P = \log(CPM_{\text{n-octanol}}/CPM_{PBS})$.

2.4. Homogenate binding

SD rats were anaesthetized with ether and killed by cervical dislocation. Their brains were rapidly removed from the skull, then the striatum regions of the brains were quickly dissected and homogenized in Tris-HCl buffer (50 mM Tris; 120 mM NaCl; pH = 7.4 adjusted with hydrochloric acid) through a high throughput homogenizer. The concentration of rat striatum homogenate was adjusted to 50 mg/mL. Each sample of rat striatum homogenate was mixed with a constant amount of ^{99m}Tc-BAT-P-DTBZ (74 KBq) and incubated at 37 °C. The blocking test was also carried out in the presence of 20 μM VMAT2 inhibitor (DTBZ). The effect of striatum amount and incubation time on the binding results was inves-

tigated. To evaluate the influencing factor on striatum amount, several different striatum homogenate solutions varying from 20 to 180 μL were added to Tris-HCl buffer containing ^{99m}Tc-BAT-P-DTBZ respectively. The mixtures were adjusted to a final volume of 0.5 mL and incubated for 2 h. In order to investigate the influencing factor on incubation time, each 100 μL of striatum homogenate was separately incubated with ^{99m}Tc-BAT-P-DTBZ in Tris-HCl buffer for 15, 30, 60, 90, 120 min. At each binding test, the basic medium and the striatum pellets bound were separated via centrifugation. The radioactivity counts of the pellets bound and the supernatant were measured by an automatic gamma counter. The striatum uptake value of ^{99m}Tc-BAT-P-DTBZ was calculated as [CPM (the pellets bound)] / [CPM (the pellets bound) + CPM (the supernatant)] × 100 % at the individual test. The blocking percentage was calculated as [Uptake Value (without inhibitor) – Uptake Value (with inhibitor)] / [Uptake Value (without inhibitor)] × 100 %.

2.5. In vivo biodistribution in normal mice

The preliminary *in vivo* experiments were conducted in accordance with the guidelines of the Animal Care and Ethics Committee of Jiangsu Institute of Nuclear Medicine. Normal mice were housed into groups for different intervals of time (30 min, 60 min, 120 min, 240 min, 360 min; n = 5 for each time point). The weight of each mouse is approximately 20–25 g. A saline solution (200 μL) of ^{99m}Tc-BAT-P-DTBZ (~7.4 MBq) was directly injected intravenously into the tail of each normal mouse. The mice (n = 5) in each group were sacrificed at the corresponding time point. The organs of interest were dissected and weighed, and then the radioactivity was measured with a γ counter. The percentage dose per gram (% ID/g ± SD) was calculated by a comparison of the organ counts to the initial injected dose.

Blocking studies were performed by coinjection (intravenous) of ^{99m}Tc-BAT-P-DTBZ (~7.4 MBq) and DTBZ (2 mg/kg) into the animals. Sixty minutes after the injection, the animals were sacrificed and their organs, including heart, liver, spleen, lung, kidney, pancreas, skin, muscle, thyroid and stomach were dissected out and the percentages of dose per gram of the samples were calculated. The ratio of target (pancreas) versus nontarget (muscle) was compared between the control and blocking groups.

2.6. Regional brain biodistribution studies

Prior to the brain biodistribution experiment, normal SD rats were housed into groups for different intervals of time (2 min, 10 min, 30 min, 60 min, 120 min; n = 5 for each time point). A total of ~ 11.1 MBq ^{99m}Tc-BAT-P-DTBZ was injected into each rat through the tail vein. At each indicated time point, the rats were executed by cervical dislocation under anaesthesia. The whole brain was quickly dissected from the skull of each rat. Different regions corresponding to cerebellum, cortex, striatum, hippocampus and midbrain were dissected and weighed from the brain. These radioactive sample were measured by an automatic gamma counter and the results were expressed as percentage of the injected dose per gram tissue in a population of five rats for each time point.

3. Results and discussion

The derivatization of DTBZ for technetium-99m labelling towards a potential VMAT2 tracer would be helpful due to the low cost, easy labelling chemistry and great availability through nuclide generator system. In the present study, a technetium-99m-labelled DTBZ derivative, ^{99m}Tc-BAT-P-DTBZ, was successfully prepared and the radiolabelling conditions were optimized. Furthermore, the biological activity of ^{99m}Tc-BAT-P-DTBZ targeting VMAT2 was also evaluated by *in vitro* and *in vivo* test.

3.1. Design and synthesis of the precursor for ^{99m}Tc-BAT-P-DTBZ

A novel combination of biologically active DTBZ vector and chelating group was developed and investigated as the precursor for ^{99m}Tc-BAT-P-DTBZ in this paper (Scheme 1). DTBZ was used as the starting material and selective demethylation of the 9-methoxy group provided the accessibility for the linkage to the desired chelator. Initially, our attempt was focused on the synthesis of the structure that the chain linker (–CH_2-CH_2CH_2-) was connected to lead DTBZ molecule before the BAT chelator attachment, but the effort of the final BAT-P-DTBZ synthesis was not successful (as shown in Fig. 3). Therefore, we tried another strategy with the chain linker coupled to the chelating group in advance. After continuous exploration, we successfully synthesized the precursor BAT-P-DTBZ (**8**) and the details were shown in Scheme 1. Firstly, DTBZ was selectively demethylated to yield 9-desmethyl-dihydrotetrabenazine (**5**) according to the literature (Kilbourn et al., 1997) and the synthesis procedure was improved. The product yield was increased (from 30 % to 75 %) by raising the reaction temperature and improving the post-treatment method. Moreover, compound **1** was alkylated by 3-bromopropanol to give a hydroxy monamide-monoamine derivant **2** and then compound **2** was tosylated by p-toluenesulfonyl chloride at 0 °C to obtain a pseudohalide **3**. Immediately, the tosylate **3** was connected to compound **5** in the presence of Cs_2CO_3 at 110 °C in DMF to generate a DTBZ derivative **6**, then the amide **6** was reduced with BH_3·THF to yield a bisaminodithiol derivative **7**. Lastly, compound **7** was deprotected with trifluoroacetic acid and methanesulfonic acid to give the precursor **8**. The instable dithiol **8** was transformed to hydrochloride salt in ether and used for the preparation of ^{99m}Tc-BAT-P-DTBZ.

3.2. Radiochemistry

The radiolabelling of compound **8** was successfully achieved according to the reported method (Meegalla et al., 1997, Zhuang et al., 1999), namely ^{99m}Tc-BAT-P-DTBZ was obtained by a simple ligand exchange reaction as shown in Scheme 2. Radiolabeling of BAT-P-DTBZ (**8**) was performed with stannous chloride as the reducing agent for the ^{99m}Tc-pertechnetate ($Na^{99m}TcO_4$). After complexation, the chelating group, BAT, formed a neutral ^{99m}Tc-TcO-BAT complex. This is a traditional technetium-99m labelling method, which has been applied successfully in the attested brain tracer ^{99m}Tc-TRODAT-1 (Huang et al., 2001). In our radiolabelling investigation, several reaction parameters, such as the reaction temperature, the reaction time, EDTA-2Na amount, GH amount,

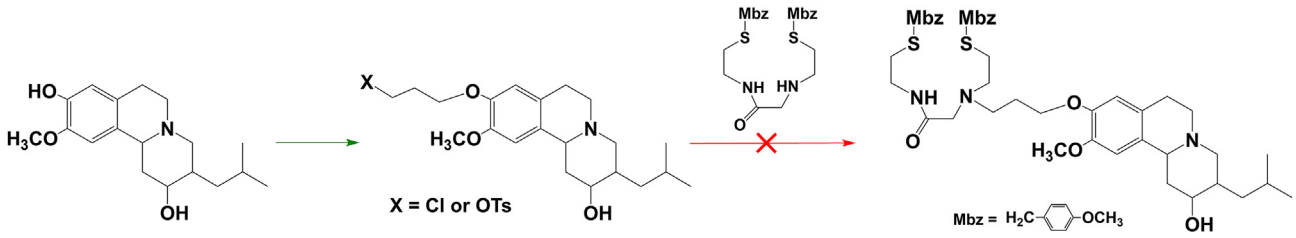

Fig. 3 The initial proposed synthesis route for the precursor BAT-P-DTBZ.

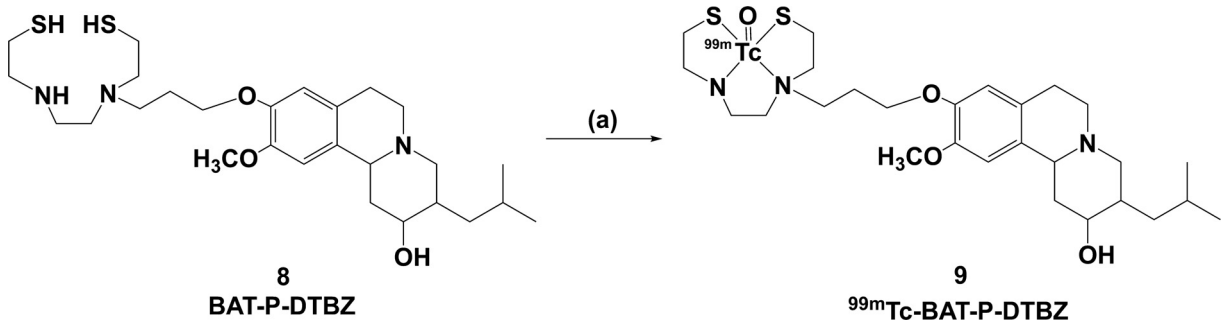

Scheme 2 Preparation of ^{99m}Tc-BAT-P-DTBZ. (a) $Na^{99m}TcO_4$, GH, $SnCl_2{\cdot}2H_2O$, EDTA-2Na, citric acid-sodium citrate buffer solution, 100 °C, 30 min.

the pH value of the reaction solution, the labelling precursor amount and $SnCl_2{\cdot}2H_2O$ amount, were investigated and optimized. For each test, only one reaction parameter was deliberately altered while fixing the other reaction parameters, and the details were shown in Table S1. The RCC was the mean value of three repeated experiments. Optimization of labelling conditions revealed that the best RCC could be achieved in the case of that labelling precursor (50 μg), $SnCl_2{\cdot}2H_2O$ (20 μg), GH (10 mg) and EDTA-2Na (1 mg) mixed at pH = 7.2 and heated in boiling water bath for 30 min.

3.2.1. Effect of the reaction temperature and time

Reaction temperature and time represent the minimum temperature and time required to achieve high RCC. Fig. 4a indicates that the RCCs are all < 90 % at 70 °C with increasing the reaction time from 5 to 30 min, indicating that the rate of formation of ^{99m}Tc-BAT-P-DTBZ complex is strongly dependent on reaction temperature. Consequently, the reaction temperature was increased to 85 °C or 100 °C, and the experimental results at the two different temperatures were basically consistent (Fig. 4b and Fig. 4c). The labelling efficiency was approximately 83 % at 5 min. After 10 min, the efficiency remained almost constant with RCC > 90 % and it reached a relative maximum of 92 % at 30 min. Consequently, 30 min was selected as the optimal reaction time. The temperature of 100 °C was chosen as the best reaction temperature due to that this temperature could be easily achieved by boiling water bath.

3.2.2. Effect of EDTA-2Na amount

Disodium edetate (EDTA-2Na) is commonly used as a stabilizer in technetium-99m labelling research (Mock and Wellman 1984, Meegalla et al., 1997, Ahlgren et al., 2010). Fig. 4d clearly depicts the effect of EDTA-2Na amount on the RCC. The radiolabelling efficiency was almost constant over the entire experiment (0.2–2 mg) and the intermediate amount (1 mg EDTA-2Na) was selected.

3.2.3. Effect of GH amount

Sodium glucoheptonate played a transitional ligand role as the form of ^{99m}Tc-GH in the preparation of ^{99m}Tc-BAT-P-DTBZ. Excess of glucoheptonate with a multi-hydroxyl moiety might facilitate the solubility of labelling precursor by dispersing the compound, and which is conducive for the ligand exchange reaction (Choi et al., 1999). Therefore, the GH amount range of 1–25 mg (much more than the amount of precursor) was investigated in our study. The effect of the GH amount was summarized in Fig. 4e. The results indicated that 10 mg GH is best for maximum RCC (approximately 95 %). The labelling efficiency was not increased significantly in the case of that the amount of GH was more than 10 mg.

3.2.4. Effect of the pH value of the reaction solution

The RCCs are influenced by the variations in pH of reaction solution as shown in Fig. 4f. At pH 2.6, the labelling efficiency was approximately 87 %. The RCCs were increased with the increase of pH. The maximum conversion was near 95 %, while pH was equal to 7.2. This phenomenon may be due to the deprotonation of the labelling precursor at a neutral pH, which is beneficial for the formation of ^{99m}Tc-BAT-P-DTBZ. With the continuous increase of pH, the labelling efficiency began to decrease. At alkaline pH value, the presence of hydroxyl ions in the reaction solution may lead to incomplete reduction of pertechnetate to the desired oxidation state and this could produce an unreliable conversion of ^{99m}Tc-BAT-P-DTBZ. Therefore, pH = 7.2 is the optimum radiolabelling condition.

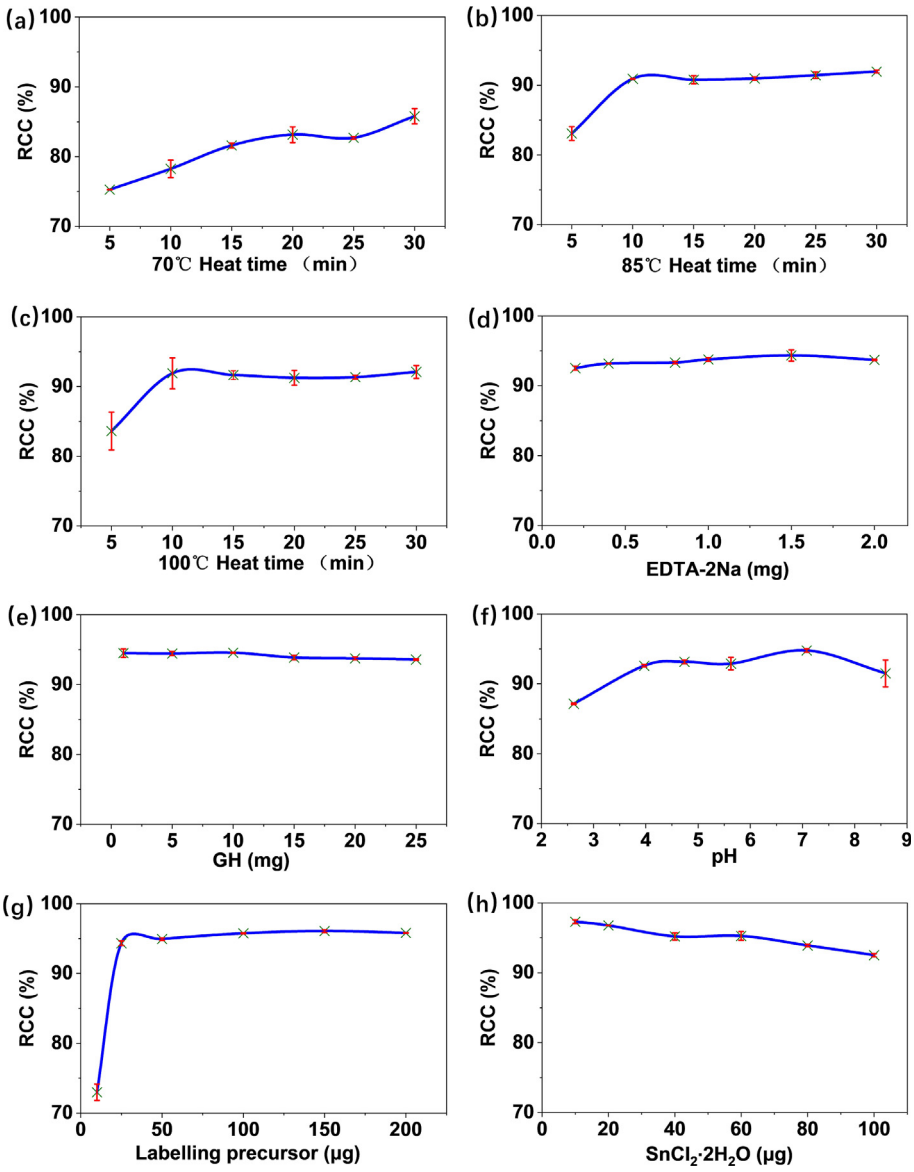

Fig. 4 Effect of reaction parameters (a. the reaction time at 70 °C; b. the reaction time at 85 °C; c. the reaction time at 100 °C; d. EDTA-2Na amount; e. GH amount; f. the pH value of the reaction solution; g. labelling precursor amount; h. $SnCl_2{\cdot}2H_2O$ amount) on the radiochemical conversion (RCC) of ^{99m}Tc-BAT-P-DTBZ.

3.2.5. Effect of labelling precursor amount

DTBZ, a bioactive molecule, was labelled with technetium-99m using the indirect technique in which the reduced technetium-99m reacted with the BAT group in the DTBZ derivative structure to form a radioactive complex. The labelling precursor amount actually influenced the RCC as shown in Fig. 4g. The reaction was carried out at different labelling precursor amounts (10–200 μg). At the low amount of precursor (< 25 μg), the RCC was relatively low due to that the precursor concentration was insufficient to form complex with all of the reduced technetium-99m. At the amount of 25–200 μg, the conversion varied in the range of 94–96 %. After comprehensive consideration, 50 μg was chosen as the optimum ligand amount required to obtain maximum RCC.

3.2.6. Effect of $SnCl_2{\cdot}2H_2O$ amount

Stannous chloride ($SnCl_2{\cdot}2H_2O$) is usually used as reducing agent for the reduction of the pertechnetate, which favors the chelation of technetium-99m with labelling precursor. Fig. 4h demonstrates the variation of the labelling efficiency with altered amount of $SnCl_2{\cdot}2H_2O$. In the whole experiment (10–100 μg), the labelling efficiency was more than 90 %. Our findings indicated that the most favorable labeling efficiency with a RCC of approximately 97 % was found at the range of 10–20 μg. At the amount of 20–100 μg, the labelling efficiency showed a slightly downward trend. This phenomenon might be explained by the formation of tin colloid (Eid Moustapha et al., 2016, Shahzadi et al., 2019). The raise of $SnCl_2{\cdot}2H_2O$ amount may lead to consume the reduced pertechnetate for the formation of ^{99m}Tc-sn-colloid, which

results in a decline in RCC of ^{99m}Tc-BAT-P-DTBZ. In this test, 10–20 μg $SnCl_2{\cdot}2H_2O$ was the optimal amount that reduced the maximum amount of pertechnetate to offer the maximum labelling efficiency. Considering the vulnerability of stannous chloride to oxidation, 20 μg $SnCl_2{\cdot}2H_2O$ was selected as the optimum amount.

3.3. Quality control

3.3.1. Radiochemical purity

Radiochemical purity of ^{99m}Tc-BAT-P-DTBZ was estimated by an HPLC method. The retention time of ^{99m}Tc-BAT-P-DTBZ was 14.9 min, while the undesirable radiochemical species such as free $^{99m}TcO_4^-$, ^{99m}Tc-radiocolloid and ^{99m}Tc-GH appeared at 1.2, 1.3 and 1.1 min, respectively. The details were depicted in the radiochromatograms (Fig. 5).

For quality control of the RCP, in addition to the undesirable radiochemical species including free $^{99m}TcO_4^-$, ^{99m}Tc-radiocolloid and ^{99m}Tc-GH, we also investigated other possible impurity of ^{99m}Tc-BAT-P-DTBZ. Ether bond could be hydrolyzed without any catalyst under high temperature (Yoon et al., 2018). The radiolabelling of compound **8** was performed through boiling water bath and the hydrolysis of phenol ether bond might occur. Probable degradation route of compound **8** was illustrated in Scheme 3A. The hydrolysis product bisaminoethanethiol-propanol (BAT-NPA) may form a possible impurity ^{99m}Tc-BAT-NPA during radiolabelling procedure. Therefore, we prepared this possible impurity as a reference (Scheme 3B). In the radiochromatogram, the retention time of ^{99m}Tc-BAT-NPA was 2.2 min as shown in Fig. 5. Fortunately, no trace of this possible impurity was observed during the preparation of ^{99m}Tc-BAT-P-DTBZ. In other words, the phenol ether bond in compound **8** is stable at ~ 100 °C.

3.3.2. Stability test

The stability of ^{99m}Tc-BAT-P-DTBZ was carried out to detect any dissociation of the title complex and to find the suitable time for the use of ^{99m}Tc-BAT-P-DTBZ to avoid the formation of undesired radiolysis product. For this purpose, ^{99m}Tc-BAT-P-DTBZ was incubated in PBS (pH = 7.4) and FBS at 37 °C for 6 h respectively. At each time point, the RCP was the mean value of three repeated measurements. The results showed that ^{99m}Tc-BAT-P-DTBZ is stable (RCP was approximately 96 %) over the period of 6 h (Fig. 6), indicating successful appositeness for the needs of late-stage biological evaluation experiments.

3.3.3. Partition coefficient

The ability of a compound to be freely across the blood–brain barrier (BBB) is related to its lipophilicity. To verify the potential of ^{99m}Tc-BAT-P-DTBZ as a brain tracer, the lipophilicity test was performed by the "shake flask" method. The technetium-99m-labelled dihydrotetrabenazine was added to a two-phase mixture of *n*-octanol and phosphate buffer and then its distribution across the two phases was determined. The results were listed in Table S2. All experiments were performed with four extractions. The values of Log$P_{7.0}$ and Log$P_{7.4}$ were found to be 1.69 ± 0.04 and 1.69 ± 0.01, respectively (n = 3, the values of the first ones in Table S2 were discarded due to the largest error). According to the literature (Dischino et al., 1983), the optimum Log*P* value for penetrating BBB is in the range of 0.9–2.5. In other words, the tracer molecules falling within this range may be free to diffuse across the BBB. Therefore, ^{99m}Tc-BAT-P-DTBZ might be suitable for permitting intercalation into the lipid bilayer of the endothelial cells and then crossing BBB.

3.4. Homogenate binding

To evaluate the biological activity of ^{99m}Tc-BAT-P-DTBZ for VMAT2, *in vitro* homogenate binding with rat striatum was performed in this study. All uptake data were presented as mean ± standard deviation (SD). Statistical differences between the experimental group and the blocking group were determined by *t*-test with Origin software. The *p*-value of < 0.05 was considered statistically significant.

As illustrated in Fig. 7a, the striatum homogenate uptake of ^{99m}Tc-BAT-P-DTBZ showed a noticeably mass-dependent increasing tendency in the range of 1–9 mg, and the uptake was decreased in the presence of VMAT2 inhibitor (DTBZ). In the experimental group, the lowest uptake of ^{99m}Tc-BAT-P-DTBZ in striatum pellets was 4.23 ± 0.15 %, while the maximum uptake was up to 13.80 ± 0.24 %. Correspondingly, the uptake of ^{99m}Tc-BAT-P-DTBZ was inhibited 33.54–44.77 %

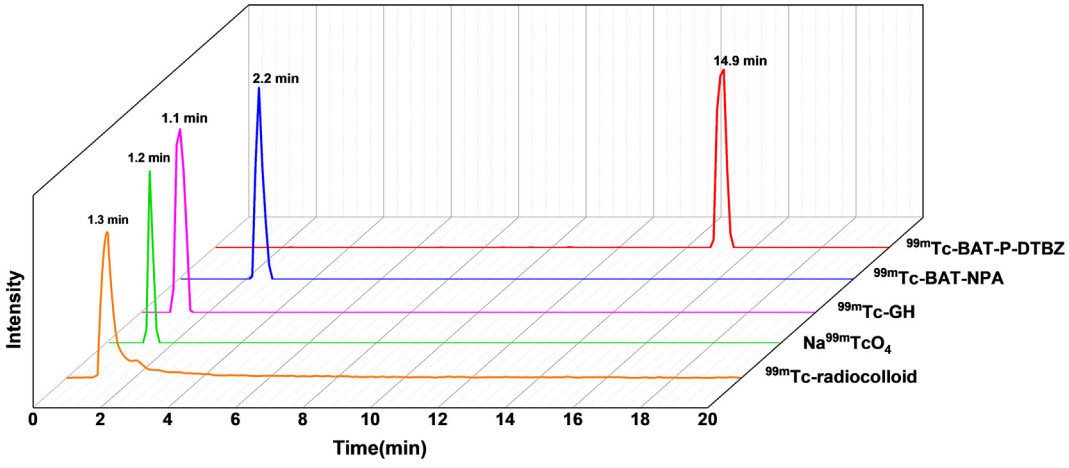

Fig. 5 Radio-HPLC chromatograms of ^{99m}Tc-BAT-P-DTBZ and its possible radiochemical impurities.

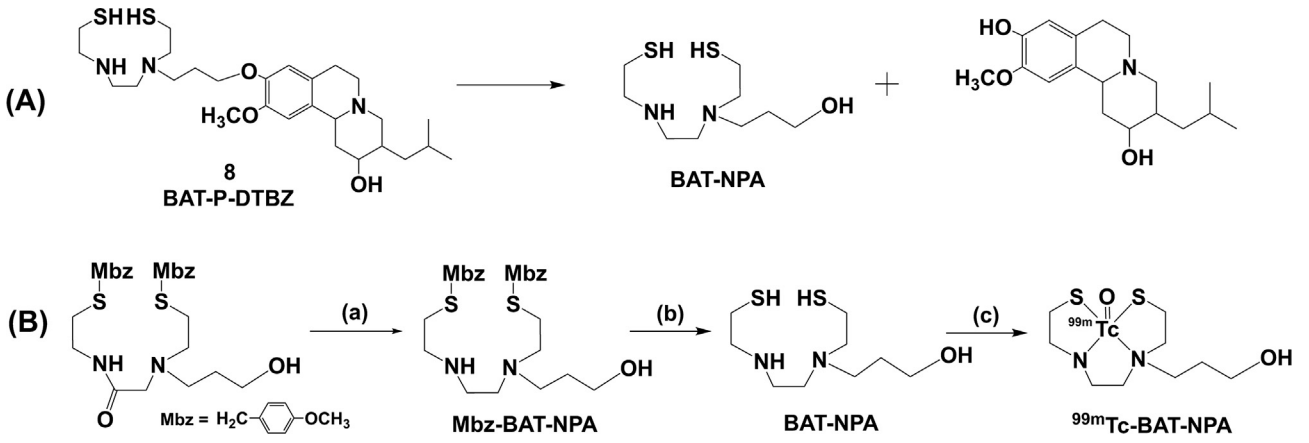

Scheme 3 (A) The hypothetical degradation route of compound **8**. (B) Preparation of ^{99m}Tc-BAT-NPA. (a) 1 M Borane-THF, 80 °C, overnight. (b) TFA, anisole, methanesulfonic acid, 0 °C to room temperature, 1 h. (c) $Na^{99m}TcO_4$, GH, $SnCl_2{\cdot}2H_2O$, EDTA-2Na, citric acid-sodium citrate buffer solution, 100 °C, 30 min.

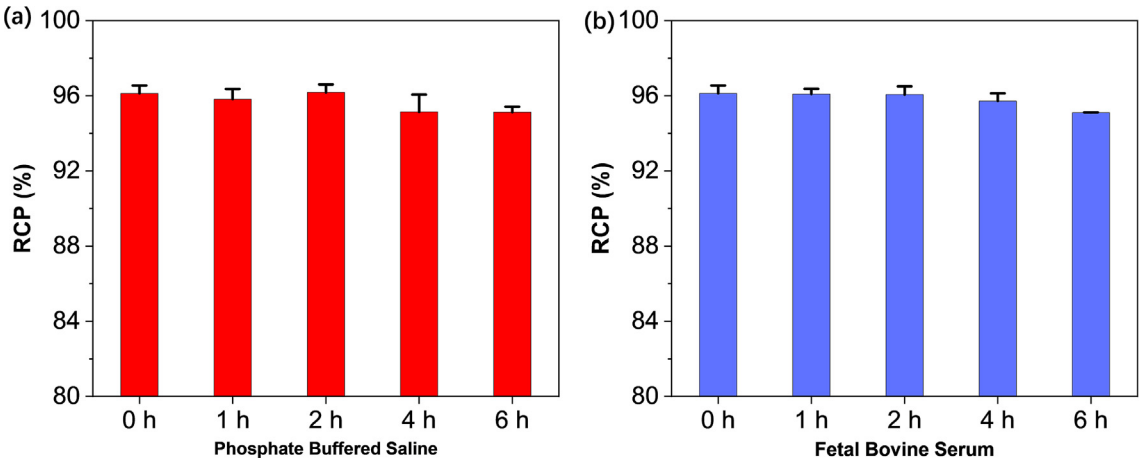

Fig. 6 *In vitro* stability of ^{99m}Tc-BAT-P-DTBZ in phosphate buffer solution (a) and fetal bovine serum (b).

by an excess of DTBZ (20 μM) in the blocking group. These results indicated that ^{99m}Tc-BAT-P-DTBZ maintains moderate specific binding affinity for VMAT2.

To further verify the effect of incubation time on the striatum binding of ^{99m}Tc-BAT-P-DTBZ, a series of time points were examined for the uptake of ^{99m}Tc-BAT-P-DTBZ in striatum pellets. The incubation time course of the uptake was shown in Fig. 7b. The uptake showed a time-dependent increasing trend within 30 min and the uptake value fluctuated between 9.88 ± 0.21 % and 12.14 ± 1.35 % at 30–120 min. The uptake of ^{99m}Tc-BAT-P-DTBZ was all decreased in the blocking test, with a 7.11 ± 0.98 % ($p < 0.05$, versus experimental group) uptake at 120 min. The above results further confirm that ^{99m}Tc-BAT-P-DTBZ could bind to VMAT2 with specificity, as well as the incubation time has a certain effect on the binding.

It is worth noting that the DTBZ used as the starting material in this study is a racemic mixture of (+) and (−) enantiomers, and the previous report shows that the *in vitro* VMAT2 binding of (±)-DTBZ is stereospecific, with a high binding affinity (K_i = 0.97 nM) for (+)-DTBZ (Kilbourn et al., 1995). Thus, an improved VMAT2 binding affinity of ^{99m}Tc-BAT-P-(+)-DTBZ should be expected, and further studies are ongoing. The present study paved the way for the development of ^{99m}Tc-BAT-P-(+)-DTBZ.

3.5. *In vivo* biodistribution in normal mice

To further verify whether our *in vitro* test was consistent with *in vivo* situation, we performed the preliminary *in vivo* biodistribution studies (Fig. 8). In our experiment, the clearance in liver was fast, while that in kidney was relatively slow. The uptake of liver and kidney was 0.29 ± 0.11 and 1.35 ± 0.03 % ID/g at the time point of 360 min, respectively. The whole brain uptake remained at a very low level throughout the biodistribution study and the uptake value decreased between 0.06 ± 0.01 and 0.02 ± 0.01 % ID/g. Moreover, the *in vivo* biodistribution study of ^{99m}Tc-BAT-P-DTBZ in mice clearly showed that the pancreas (target, VMAT2-enriched region) displays the highest uptake (1.55 ± 0.14 % ID/g) with the exception of kidney in the body at 60 min after injection as shown in Fig. 8. Furthermore, important requirement for pan-

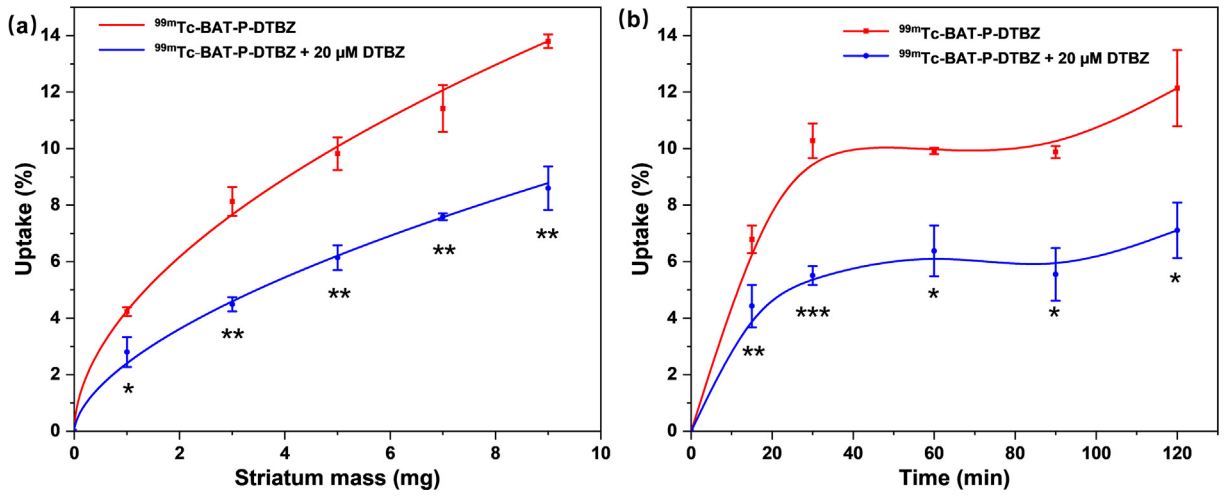

Fig. 7 *In vitro* striatum homogenate binding and blocking assays of ^{99m}Tc-BAT-P-DTBZ in Tris-HCl buffer solution. (a) Striatum mass-uptake curve of ^{99m}Tc-BAT-P-DTBZ. Results are means ± SD of three independent measurements (n = 3). (b) Incubation time-uptake curve of ^{99m}Tc-BAT-P-DTBZ. Results are means ± SD of three independent measurements (n = 3). The uptake data were analyzed by *t*-test. *, $p < 0.05$; **, $p < 0.01$; ***, $p < 0.001$ (blocking group versus experimental group).

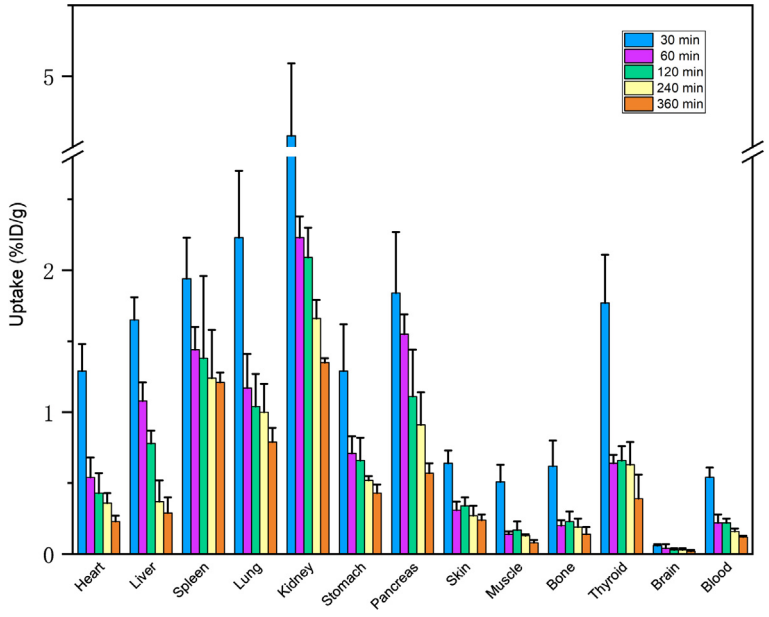

Fig. 8 Biodistribution of ^{99m}Tc-BAT-P-DTBZ in mice. The data were expressed as the percentage of injected dose per gram of tissue (% ID/g, n = 5, mean ± SD).

creatic VMAT2 imaging agents involves the avoidance of accumulation in organs located near the pancreas. Since the off-target accumulation in organs located near the pancreas impairs the signal–noise ratio. Especially, the liver is located very close to the pancreas. In our study, the liver showed a low uptake (1.08 ± 0.13 % ID/g) at the time point of 60 min. The ratio of pancreas to liver was approximately 1.43, and this ratio obtained with ^{99m}Tc-BAT-P-DTBZ is consistent with the reported ratio of pancreas to liver (~1.50) in rats at 60 min for [^{11}C]DTBZ (Fagerholm et al., 2010). These results indicated that ^{99m}Tc-BAT-P-DTBZ has a high potential to serve as a radiotracer for VMAT2 imaging in pancreas. It was worth noting that the spleen demonstrated a relatively high uptake in the entire experiment cycle. This phenomenon may be related to a trace of impurity (^{99m}Tc-radiocolloid) in ^{99m}Tc-BAT-P-DTBZ.

To confirm that the pancreas uptake is specifically due to the VMAT2 signal, blocking studies were performed via coadministration with VMAT2 inhibitor DTBZ. In this experiment, the pancreas uptake was blocked by the competing dose of DTBZ (2 mg/kg) as detailed in Fig. 9. Statistical differences between the control and blocking group were evaluated by *t*-test. In the control group, the ratio of target/non-target (pancreas/muscle) was approximately 11.51. Coadministration with DTBZ resulted in a significant blocking of the uptake in the pancreas (~30 %), with a target/non-target ratio of

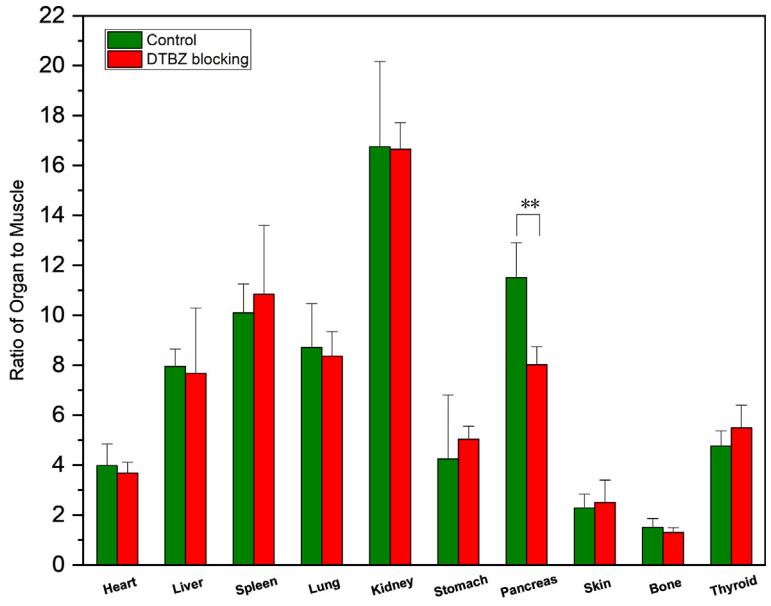

Fig. 9 In vivo blocking assays of ^{99m}Tc-BAT-P-DTBZ in mice. Data were obtained at 60 min post injection and presented as the mean ± SD, n = 5. **, $p < 0.01$ versus control group.

8.02 ± 0.72 ($p < 0.01$, n = 5) remaining at 60 min after injection. The blocking effect was comparable with the literature (Kung et al., 2008b). Thus, in this study, the specific VMAT2 binding signal was detected in the *in vivo* pancreas.

To compare the biological distribution differences between ^{99m}Tc-BAT-P-DTBZ and ^{99m}Tc-pertechnetate, we also carried out the biodistribution of pertechnetate solution as negative control (Fig. 10). The *in vivo* biodistribution study of ^{99m}Tc-pertechnetate in mice clearly showed that the thyroid exhibits the highest uptake (64.56 ± 4.89 % ID/g) in the body at 60 min after injection. Our experimental results were similar to those in the literature (Jang et al., 2022). Compared with pure technetium-99m, the uptake value of stomach, thyroid and blood was very low in the biodistribution of ^{99m}Tc-BAT-P-DTBZ.

3.6. Regional brain biodistribution studies

In order to evaluate the specific uptake of ^{99m}Tc-BAT-P-DTBZ in the *in vivo* brain, regional brain biodistribution studies were carried out with SD rats. Unfortunately, the investigation indicated that the whole rat brain uptake is poor at each time point and the values are far from that of the attested brain tracer ^{99m}Tc-TRODAT-1 (Meegalla et al., 1997) (0.024 ± 0.

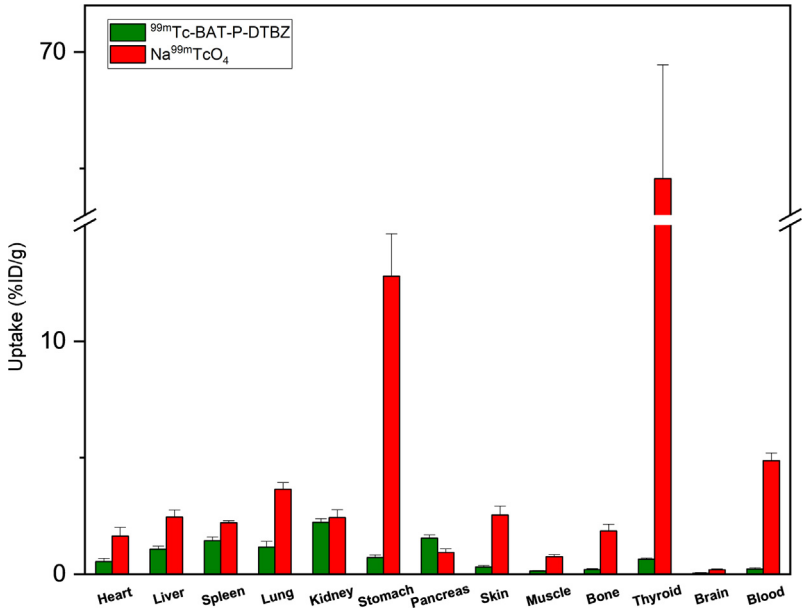

Fig. 10 Biodistribution of ^{99m}Tc-pertechnetate and ^{99m}Tc-BAT-P-DTBZ in mice. Data were obtained at 60 min post injection and presented as the mean ± SD, n = 5.

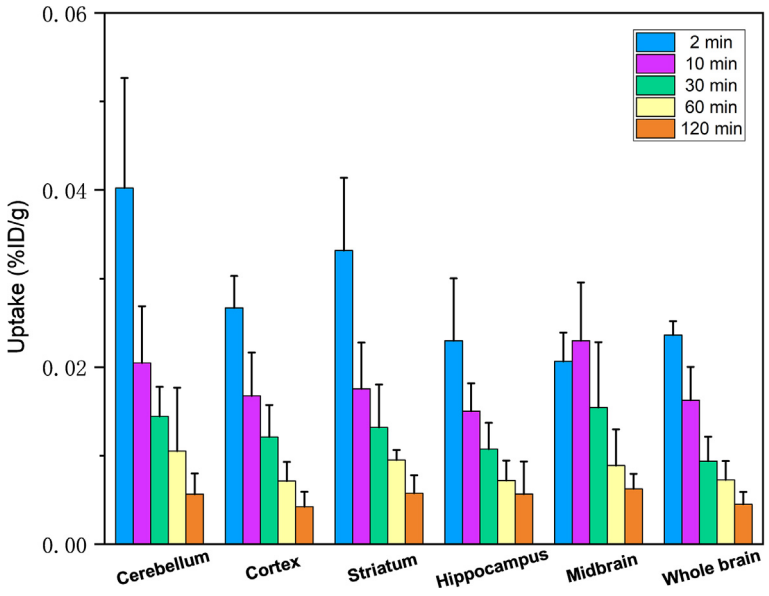

Fig. 11 Regional brain biodistribution of ^{99m}Tc-BAT-P-DTBZ in rats. The data were expressed as the percentage of injected dose per gram of tissue (% ID/g, n = 5, mean ± SD).

002 vs 0.43 ± 0.16 % ID/g, 2 min; 0.007 ± 0.002 vs 0.12 ± 0. 001 % ID/g, 60 min). As shown in Fig. 11, no obvious concentration was found in the target area (striatum) due to the weak brain uptake. Although the lipophilicity test showed that ^{99m}Tc-BAT-P-DTBZ might be suitable for crossing into the brain, the brain biodistribution revealed an inability to penetrate BBB. This was probably caused by several reasons. On the one side, the title complex might be a target for active efflux transporters such as P-glycoprotein (Cordon-Cardo et al., 1989) or other multidrug resistance proteins (Lingineni et al., 2017). On the other side, the lipophilicity of the title tracer might not be good enough to permit intercalation into the lipid bilayer of the endothelial cells. Based on the *in vivo* biodistribution and regional brain biodistribution in animals, ^{99m}Tc-BAT-P-DTBZ has a potential for non-invasive assessment of VMAT2 in pancreas or other non-brain organs.

4. Conclusion

To develop a radiometal-labelled DTBZ for VMAT2 tracing, a novel ^{99m}Tc-BAT-P-DTBZ was designed and prepared in this report. Furthermore, the *in vitro* and *in vivo* biological evaluation revealed that ^{99m}Tc-BAT-P-DTBZ offers potential for VMAT2 tracing in pancreas organ. Therefore, we successfully derivatized the lead DTBZ molecule for technetium-99m radiolabelling without compromising its VMAT2 binding affinity in the present study.

Declaration of Competing Interest

The authors declare that they have no known competing financial interests or personal relationships that could have appeared to influence the work reported in this paper.

Acknowledgments

The present work was supported by the Research Foundation of Jiangsu Provincial Commission of Health (M2022047), the National Natural Science Foundation of China (82172054) and the Natural Science Foundation of Jiangsu Province (BK20201133, BK20210062).

Appendix A. Supplementary material

Supplementary data to this article can be found online at https://doi.org/10.1016/j.arabjc.2023.104572.

References

Ahlgren, S., Andersson, K., Tolmachev, V., 2010. Kit formulation for ^{99m}Tc-labeling of recombinant anti-HER2 Affibody molecules with a C-terminally engineered cysteine. Nucl. Med. Biol. 37, 539–546. https://doi.org/10.1016/j.nucmedbio.2010.02.009.

Bernstein, A.I., Stout, K.A., Miller, G.W., 2014. The vesicular monoamine transporter 2: an underexplored pharmacological target. Neurochem. Int. 73, 89–97. https://doi.org/10.1016/j.neuint.2013.12.003.

Chan, G.L.Y., Holden, J.E., Stoessl, A.J., Samii, A., Doudet, D.J., Dobko, T., Morrison, K.S., Adam, M., Schulzer, M., Calne, D.B., Ruth, T.J., 1999. Reproducibility studies with ^{11}C-DTBZ, a monoamine vesicular transporter inhibitor in healthy human subjects. J. Nucl. Med. 40, 283–289.

Choi, S.R., Kung, M.P., Plössl, K., Meegalla, S., Kung, H.F., 1999. An improved kit formulation of a dopamine transporter imaging agent: [Tc-99m]TRODAT-1. Nucl. Med. Biol. 26, 461–466. https://doi.org/10.1016/S0969-8051(99)00010-4.

Cliburn, R.A., Dunn, A.R., Stout, K.A., Hoffman, C.A., Lohr, K.M., Bernstein, A.I., Winokur, E.J., Burkett, J., Schmitz, Y., Caudle, W. M., Miller, G.W., 2017. Immunochemical localization of vesicular monoamine transporter 2 (VMAT2) in mouse brain. J. Chem. Neuroanat. 83–84, 82–90. https://doi.org/10.1016/j.jchemneu.2016.11.003.

Cordon-Cardo, C., O'Brien, J.P., Casals, D., Rittman-Grauer, L., Biedler, J.L., Melamed, M.R., Bertino, J.R., 1989. Multidrug-resistance gene (P-glycoprotein) is expressed by endothelial cells at blood-brain barrier sites. Proc. Natl. Acad. Sci. 86, 695–698. https://doi.org/10.1073/pnas.86.2.695.

Davoodikia, B., Hamedani, M.P., Saffari, M., Ebrahimi, S.E.S., Seyyed, H., Hashemi, S., Ardestani, M.S., Ghoreishi, S.M., 2022.

Synthesis of novel nano-radiotracer for in-vivo bone imaging: 99mTc- citric acid based PEG dendrimer and its conjugation with alendronate. Arabian J. Chem. 15, 104060. https://doi.org/10.1016/j.arabjc.2022.104060.

Dischino, D.D., Welch, M.J., Kilbourn, M.R., Raichle, M.E., 1983. Relationship Between Lipophilicity and Brain Extraction of C-11-Labeled Radiopharmaceuticals. J. Nucl. Med. 24, 1030–1038.

Eid Moustapha, M., Shweeta, H.A., Motaleb, M.A., 2016. Technetium-labeled danofloxacin complex as a model for infection imaging. Arabian J. Chem. 9, S1928–S1934. https://doi.org/10.1016/j.arabjc.2014.10.017.

Eriksson, O., Jahan, M., Johnström, P., Korsgren, O., Sundin, A., Halldin, C., Johansson, L., 2010. In vivo and in vitro characterization of [^{18}F]-FE-(+)-DTBZ as a tracer for beta-cell mass. Nucl. Med. Biol. 37, 357–363. https://doi.org/10.1016/j.nucmedbio.2009.12.004.

Fagerholm, V., Mikkola, K.K., Ishizu, T., Arponen, E., Kauhanen, S., Någren, K., Solin, O., Nuutila, P., Haaparanta, M., 2010. Assessment of islet specificity of dihydrotetrabenazine radiotracer binding in rat pancreas and human pancreas. J. Nucl. Med. 51, 1439–1446. https://doi.org/10.2967/jnumed.109.074492.

Freeby, M.J., Kringas, P., Goland, R.S., Leibel, R.L., Maffei, A., Divgi, C., Ichise, M., Harris, P.E., 2016. Cross-sectional and Test-Retest Characterization of PET with [^{18}F]FP-(+)-DTBZ for β Cell Mass Estimates in Diabetes. Mol. Imaging Biol. 18, 292–301. https://doi.org/10.1007/s11307-015-0888-7.

Frey, K.A., Koeppe, R.A., Kilbourn, M.R., Vander Borght, T.M., Albin, R.L., Gilman, S., Kuhl, D.E., 1996. Presynaptic monoaminergic vesicles in Parkinson's disease and normal aging. Ann. Neurol. 40, 873–884. https://doi.org/10.1002/ana.410400609.

Goswami, R., Ponde, D.E., Kung, M.-P., Hou, C., Kilbourn, M.R., Kung, H.F., 2006. Fluoroalkyl derivatives of dihydrotetrabenazine as positron emission tomography imaging agents targeting vesicular monoamine transporters. Nucl. Med. Biol. 33, 685–694. https://doi.org/10.1016/j.nucmedbio.2006.05.006.

Harris, P.E., Ferrara, C., Barba, P., Polito, T., Freeby, M., Maffei, A., 2008. VMAT2 gene expression and function as it applies to imaging β-cell mass. J. Mol. Med. 86, 5–16. https://doi.org/10.1007/s00109-007-0242-x.

Hoffman, B.J., Hansson, S.R., Mezey, É., Palkovits, M., 1998. Localization and dynamic regulation of biogenic amine transporters in the mammalian central nervous system. Front. Neuroendocrinol. 19, 187–231. https://doi.org/10.1006/frne.1998.0168.

Hsiao, I.-T., Weng, Y.-H., Hsieh, C.-J., Lin, W.-Y., Wey, S.-P., Kung, M.-P., Yen, T.-C., Lu, C.-S., Lin, K.-J., 2014. Correlation of parkinson disease severity and ^{18}F-DTBZ positron emission tomography. JAMA Neurol. 71, 758–766. https://doi.org/10.1001/jamaneurol.2014.290.

Huang, W.-S., Lin, S.-Z., Lin, J.-C., Wey, S.-P., Ting, G., Liu, R.-S., 2001. Evaluation of Early-Stage Parkinson's Disease with ^{99m}Tc-TRODAT-1 Imaging. J. Nucl. Med. 42, 1303–1308.

Jang, J., Kumakura, Y., Tatenuma, K., Ozeki, A.N., Wada, Y., Akimitsu, N., Tsuguchi, A., Kikunaga, H., Higaki, S., Uesaka, M., 2022. A preliminary biodistribution study of [99mTc]sodium pertechnetate prepared from an electron linear accelerator and activated carbon-based 99mTc generator. Nucl. Med. Biol. 110–111, 1–9. https://doi.org/10.1016/j.nucmedbio.2022.03.002.

Kilbourn, M.R., 1997. In vivo radiotracers for vesicular neurotransmitter transporters. Nucl. Med. Biol. 24, 615–619. https://doi.org/10.1016/S0969-8051(97)00101-7.

Kilbourn, M., Lee, L., Borght, T.V., Jewett, D., Frey, K., 1995. Binding of α-dihydrotetrabenazine to the vesicular monoamine transporter is stereospecific. Eur. J. Pharmacol. 278, 249–252. https://doi.org/10.1016/0014-2999(95)00162-E.

Kilbourn, M.R., Lee, L.C., Heeg, M.J., Jewett, D.M., 1997. Absolute configuration of (+)-α-dihydrotetrabenazine, an active metabolite of tetrabenazine. Chirality. 9, 59–62. https://doi.org/10.1002/(SICI)1520-636X(1997)9:1<59::AID-CHIR11>3.0.CO;2-P.

Koeppe, R.A., Frey, K.A., Vander Borght, T.M., Karlamangla, A., Jewett, D.M., Lee, L.C., Kilbourn, M.R., Kuhl, D.E., 1996. Kinetic Evaluation of [^{11}C]Dihydrotetrabenazine by dynamic PET: measurement of vesicular monoamine transporter. J. Cereb. Blood Flow Metab. 16, 1288–1299. https://doi.org/10.1097/00004647-199611000-00025.

Kumar, A., Lo, S.-T., Öz, O.K., Sun, X., 2014. Derivatization of (±) dihydrotetrabenazine for copper-64 labeling towards long-lived radiotracers for PET imaging of the vesicular monoamine transporter 2. Bioorg. Med. Chem. Lett. 24, 5663–5665. https://doi.org/10.1016/j.bmcl.2014.10.070.

Kung, M.-P., Hou, C., Goswami, R., Ponde, D.E., Kilbourn, M.R., Kung, H.F., 2007. Characterization of optically resolved 9-fluoropropyl-dihydrotetrabenazine as a potential PET imaging agent targeting vesicular monoamine transporters. Nucl. Med. Biol. 34, 239–246. https://doi.org/10.1016/j.nucmedbio.2006.12.005.

Kung, M.-P., Hou, C., Lieberman, B.P., Oya, S., Ponde, D.E., Blankemeyer, E., Skovronsky, D., Kilbourn, M.R., Kung, H.F., 2008b. In vivo imaging of β-Cell mass in rats using ^{18}F-FP-(+)-DTBZ: a potential PET ligand for studying diabetes mellitus. J. Nucl. Med. 49, 1171–1176. https://doi.org/10.2967/jnumed.108.051680.

Kung, H.F., Lieberman, B.P., Zhuang, Z.-P., Oya, S., Kung, M.-P., Choi, S.R., Poessl, K., Blankemeyer, E., Hou, C., Skovronsky, D., Kilbourn, M., 2008a. In vivo imaging of vesicular monoamine transporter 2 in pancreas using an ^{18}F epoxide derivative of tetrabenazine. Nucl. Med. Biol. 35, 825–837. https://doi.org/10.1016/j.nucmedbio.2008.08.004.

Lin, K.-J., Lin, W.-Y., Hsieh, C.-J., Weng, Y.-H., Wey, S.-P., Lu, C.-S., Skovronsky, D., Yen, T.-C., Chang, C.-J., Kung, M.-P., Hsiao, I.-T., 2011. Optimal scanning time window for ^{18}F-FP-(+)-DTBZ (^{18}F-AV-133) summed uptake measurements. Nucl. Med. Biol. 38, 1149–1155. https://doi.org/10.1016/j.nucmedbio.2011.05.010.

Lingineni, K., Belekar, V., Tangadpalliwar, S.R., Garg, P., 2017. The role of multidrug resistance protein (MRP-1) as an active efflux transporter on blood–brain barrier (BBB) permeability. Mol. Divers. 21, 355–365. https://doi.org/10.1007/s11030-016-9715-6.

Liu, C., Chen, Z., Li, X., Tang, J., 2012a. A concise synthesis of tetrabenazine and its crystal structure. Mol. Cryst. Liq. Cryst. 557, 39–49. https://doi.org/10.1080/15421406.2011.627764.

Liu, C., Chen, Z., Li, X., Tang, J., 2012b. Synthesis and X-ray analysis of dihydrotetrabenazine, a metabolite of tetrabenazine. Mol. Cryst. Liq. Cryst. 562, 191–199. https://doi.org/10.1080/15421406.2012.661315.

Liu, F., Choi, S.R., Zha, Z., Ploessl, K., Zhu, L., Kung, H.F., 2018. Deuterated ^{18}F–9-O-hexadeutero-3-fluoropropoxyl-(+)-dihydrotetrabenazine (D6-FP-(+)-DTBZ): a vesicular monoamine transporter 2 (VMAT2) imaging agent. Nucl. Med. Biol. 57, 42–49. https://doi.org/10.1016/j.nucmedbio.2017.11.009.

Liu, C., Tang, J., Xu, Y., Cao, S., Fang, Y., Zhao, C., Chen, Z., 2021. Molar activity of [^{18}F]FP-(+)-DTBZ radiopharmaceutical: Determination and its effect on quantitative analysis of VMAT2 autoradiography. J. Pharm. Biomed. Anal. 203,. https://doi.org/10.1016/j.jpba.2021.114212 114212.

Lohr, K.M., Stout, K.A., Dunn, A.R., Wang, M., Salahpour, A., Guillot, T.S., Miller, G.W., 2015. Increased vesicular monoamine transporter 2 (VMAT2; Slc18a2) protects against methamphetamine toxicity. ACS Chem. Neurosci. 6, 790–799. https://doi.org/10.1021/acschemneuro.5b00010.

Maffei, A., Liu, Z., Witkowski, P., Moschella, F., Pozzo, G.D., Liu, E., Herold, K., Winchester, R.J., Hardy, M.A., Harris, P.E., 2004. Identification of tissue-restricted transcripts in human islets. Endocrinology. 145, 4513–4521. https://doi.org/10.1210/en.2004-0691.

Meegalla, S.K., Plössl, K., Kung, M.-P., Chumpradit, S., Stevenson, D.A., Kushner, S.A., McElgin, W.T., Mozley, P.D., Kung, H.F., 1997. Synthesis and characterization of technetium-99m-labeled

tropanes as dopamine transporter-imaging agents. J. Med. Chem. 40, 9–17. https://doi.org/10.1021/jm960532j.

Mock, B.H., Wellman, H.N., 1984. Stoichiometric Tc-99m RBC labeling using stable kit solutions of stannous chloride and EDTA: concise communication. J. Nucl. Med. 25, 881–886.

Mogadam, H.Y., Erfani, M., Nikpassand, M., Mokhtary, M., 2020. Preparation and assessment of a new radiotracer technetium-99m-6-hydrazinonicotinic acid-tyrosine as a targeting agent in tumor detecting through single photon emission tomography. Bioorg. Chem. 104,. https://doi.org/10.1016/j.bioorg.2020.104181 104181.

Mogadam, H.Y., Erfani, M., Nikpassand, M., Mokhtary, M., 2022. Evaluation of [^{99m}Tc][Tc-HYNIC/EDDA]-Tyr as a target for metabolic tumor imaging in B16F10 melanoma tumor. Asia Oceania J. Nucl. Med. Biol. 10, 100–108. https://doi.org/10.22038/aojnmb.2021.60334.1420.

Nag, S., Jahan, M., Tóth, M., Nakao, R., Varrone, A., Halldin, C., 2021. PET Imaging of VMAT2 with the novel Radioligand [^{18}F]FE-DTBZ-d4 in nonhuman primates: comparison with [^{11}C]DTBZ and [^{18}F]FE-DTBZ. ACS Chem. Neurosci. 12, 4580–4586. https://doi.org/10.1021/acschemneuro.1c00651.

O'Neil, J.P., Wilson, S.R., Katzenellenbogen, J.A., 1994. Preparation and structural characterization of monoamine-monoamide bis (thiol) oxo complexes of technetium(V) and rhenium(V). Inorg. Chem. 33, 319–323. https://doi.org/10.1021/ic00080a022.

Sanchez-Catasus, C.A., Bohnen, N.I., Yeh, F.-C., D'Cruz, N., Kanel, P., Müller, M.L.T.M., 2021. Dopaminergic nigrostriatal connectivity in early parkinson disease. in vivo neuroimaging study of ^{11}C-DTBZ PET combined with correlational tractography. J. Nucl. Med. 62, 545–552. https://doi.org/10.2967/jnumed.120.248500.

Shahzad, S., Qadir, M.A., Rasheed, R., Ahmed, M., 2019. Synthesis of ^{99m}Tc-gemifloxacin freeze dried kits and their biodistribution in Salmonella typhi, Pseudomonas aeruginosa and Klebsiella pneumoniae. Arabian J. Chem. 12, 664–670. https://doi.org/10.1016/j.arabjc.2015.10.002.

Shahzadi, S.K., Qadir, M.A., Shabnam, S., Javed, M., 2019. ^{99m}Tc-amoxicillin: a novel radiopharmaceutical for infection imaging. Arabian J. Chem. 12, 2533–2539. https://doi.org/10.1016/j.arabjc.2015.04.003.

Simpson, N.R., Souza, F., Witkowski, P., Maffei, A., Raffo, A., Herron, A., Kilbourn, M., Jurewicz, A., Herold, K., Liu, E., Hardy, M.A., Van Heertum, R., Harris, P.E., 2006. Visualizing pancreatic β-cell mass with [^{11}C]DTBZ. Nucl. Med. Biol. 33, 855–864. https://doi.org/10.1016/j.nucmedbio.2006.07.002.

Yoon, J., Sim, S., Myint, A.A., Lee, Y.-W., 2018. Kinetics of the hydrolysis of xylan based on ether bond cleavage in subcritical water. J. Supercritical Fluids 135, 145–151. https://doi.org/10.1016/j.supflu.2018.01.013.

Zhao, C., Liu, C., Tang, J., Xu, Y., Xie, M., Chen, Z., 2020. An efficient automated radiosynthesis and bioactivity confirmation of VMAT2 Tracer [^{18}F]FP-(+)-DTBZ. Mol. Imaging Biol. 22, 265–273. https://doi.org/10.1007/s11307-019-01379-6.

Zhuang, Z.-P., Plössl, K., Kung, M.-P., Mu, M., Kung, H.F., 1999. Neutral and stereospecific Tc-99m complexes: [^{99m}Tc]N-benzyl-3,4-di-(N-2-mercaptoethyl)-amino-pyrrolidines (P-BAT). Nucl. Med. Biol. 26, 217–224. https://doi.org/10.1016/S0969-8051(98)00099-7.